Radio Science, Volume 30, Number 4, Pages 961–973, July–August 1995

Fine structure of the auroral kilometric radiation: A Fermi acceleration process?

W. M. Farrell

Laboratory for Extraterrestrial Physics, NASA Goddard Space Flight Center, Greenbelt, Maryland

Abstract. The fine structure of the auroral kilometric radiation is explained as a nonlinear interaction between the locally generated cyclotron emission created in an electron plasma cavity and the cavity boundary. Specifically, it is demonstrated that broadband cyclotron emission can form discrete tones after numerous interactions with an oscillating boundary that has quasi-monochromatic wavelike motion. This boundary will Doppler shift most radio photons in a stochastic way, creating a diffuse background radio component. However, some radio photons will have regular, stable frequencies that form discrete tones that overlie on the diffuse background emission. The discrete tones are created in situations where the photon travel time in the cavity is an integer multiple of the boundary oscillation period, this effect establishing a resonance between the boundary oscillations and photon. A set of coupled nonlinear equations is used to describe the radio photon/cavity boundary interaction. Effects of wave growth in the local density cavity and boundary reflections are also included. As the character of the cavity slowly changes, the resonance condition also changes in an adiabatic way, shifting the resonance to different frequencies. The net result is the creation of drifting radio tones which are comparable to those actually observed on radio spectrograms of the auroral kilometric radiation.

Introduction

In this paper a theory is presented to explain the very interesting fine structure observed with the Earth's auroral kilometric radiation (AKR) [*Gurnett et al.*, 1979]. The AKR is an intense radio emission commonly observed between 100 kHz and 600 kHz by radio instruments onboard Earth-orbiting spacecraft [*Dunkel et al.*, 1970]. The emission originates from the nightside terrestrial auroral region between 1.4 and 3 R_E [*Gurnett*, 1974] and is generated by the same energetic electrons responsible for discrete UV auroral arcs [*Benson et al.*, 1980; *Huff et al.*, 1988]. The emitted kilometric radio power from the auroral region is typically about 10^7 W [*Gallagher and Gurnett*, 1979] but at times can become as large as 10^9 W [*Gurnett*, 1974]. The AKR is most intense during magnetospherically disturbed periods [*Gurnett*, 1974]. Thus the emission is a good indicator of magnetospheric and auroral activity [*Kaiser and Alexander*, 1977].

There have been an abundance of theories proposed to explain the generation of AKR. However, the most widely accepted theory for emission generation is the stimulated amplification of background radiation via a cyclotron resonance interaction with suprathermal electrons [*Melrose*, 1976; *Wu and Lee*, 1979]. This theory explains many gross features of the emission including its generation near the local cyclotron frequency, most of its radiated power [*Omidi and Gurnett*, 1982], the presence of both strong extraordinary and weak ordinary mode emission [*Wu and Lee*, 1979], and radiation beamed at relatively large angles with respect to the local magnetic field [*Calvert*, 1981a].

Wu and Lee [1979] analytically demonstrated that cyclotron emission can be generated from a loss cone suprathermal electron distribution. In this case, wave growth occurs in electron velocity phase space regions where the distribution $F(v_\parallel, v_\perp)$ has a positive slope in the perpendicular velocity component: $\partial F/\partial v_\perp > 0$. *Omidi and Gurnett* [1982] used measured S3-3 electron distributions and found that large cyclotron wave growth was possible from both the loss cone feature and "hole" in the electron distribution. *Louarn et al.* [1990] suggested that the cyclotron emission is generated by the trapped electrons found between the mirror point

Paper number 95RS00832.

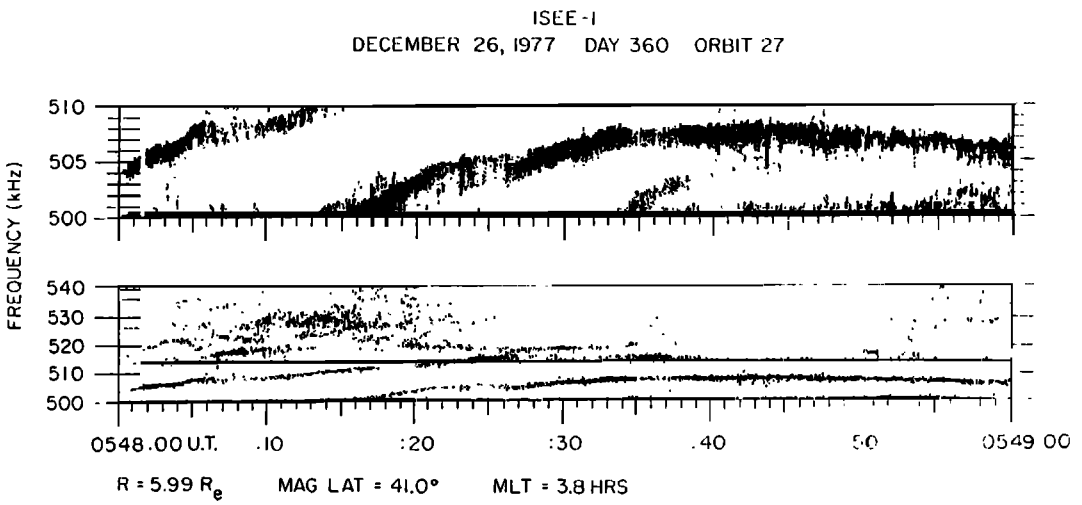

Figure 1. A frequency-versus-time spectrogram obtained from the ISEE 1 wideband waveform receiver showing the AKR fine structure in a (top) 10-kHz and (bottom) 40-kHz bandpass. Figure adapted from *Gurnett and Anderson* [1981].

below the spacecraft and a field-aligned potential region above the spacecraft. *Fung and Viñas* [1994] demonstrate that very strong cyclotron wave amplification can occur in regions where the electrostatic potential drop along the field line is large, thereby creating a hole or large dropout in the electron distribution favorable for wave growth.

The above-cited theories may explain the macroscopic character of the emission. However, a most interesting feature of the AKR is its fine structure. Most sweep frequency receivers sample measurements in a relatively broad band pass. Further, temporal averaging of the data is performed in the sweep frequency receiver circuitry, reducing the time resolution of the measurement. Thus, the microscopic spectral properties of AKR are not quantified. However, spacecraft like ISEE 1 and 2 and DE 1 flew waveform receivers that sampled the measured antenna voltage in a given band pass at the Nyquist frequency. Spectral analysis of these waveforms occurs on the ground. Such waveform analysis of AKR proves quite revealing. Figure 1, from *Gurnett and Anderson* [1981], shows a dynamic spectrogram obtained by Fourier transforming the original waveform. At high temporal and spectral resolution AKR appears to consist of discrete tones that drift both upward and downward in frequency. The discrete tones are often observed as sets which drift as a group at nearly the same rate, although more complicated structure is also observed.

Clearly, an added ingredient is required to the proposed cyclotron emission theories in order to explain the observed discrete features. Specifically, each of the above-cited theories would predict a rather broadbanded, continuous emission from the auroral region, and not the observed narrowbanded tones. To explain the tones, *Gurnett and Anderson* [1981] suggested that a slow-moving ion disturbance is passing through the AKR source region. This disturbance would concentrate electrons and enhance the stimulated emission process in that region. *Melrose* [1986], using a VLF whistler analogy, suggested that the intense AKR signals beamed outward from the auroral region would bunch electrons in the incoming streams. Radiation from such bunches would then appear as discrete tones. *McKean and Winglee* [1991] suggested that the fine structure of AKR results from the superposition of radio packets originating from different locations along the active field line. *Pritchett and Winglee* [1989] performed a simulation of the auroral radio and plasma wave process using a suprathermal loss cone electron stream. An unexpected result was the formation of discrete tones in the freely propagating cyclotron emission generated from the simulated beam. A concept that is gaining acceptance in the community is the laser mechanism for AKR gener-

ation [*Calvert*, 1982]. It was demonstrated that amplification and entrainment of the AKR signals can occur at locations along the magnetic field line where the emission wavelength, λ, is an integer multiple of the density inhomogeneity width, $L = m\lambda$. As the size of the field-aligned inhomogeneity changes, the locations satisfying the entrainment criteria will also change (i.e., move up or down the field line), resulting in a drifting of the discrete tones. To date, no single model for the fine structure has gained a consensus opinion in the community. However, there is considerable evidence indicating that the AKR generation process is indeed laserlike [*Farrell and Gurnett*, 1985; *Farrell et al.*, 1986; *Baumback and Calvert*, 1987], as originally formulated by *Calvert* [1982].

Besides the above-described processes, there is also another way of obtaining very discrete tones in a trapped system. Specifically, if one or both of the boundaries (i.e., density depletion walls) are oscillating, a new entrainment condition acts to form discrete tones in an initially broadband disturbance. This condition requires that the wave's group travel time in the cavity be an integer ratio of the boundary oscillation period. When this condition is satisfied, a resonance between the photon and boundary occurs. In this paper we examine the AKR emitted from an active site in an auroral plasma cavity. We assume the AKR is locally generated in a quasi-perpendicular mode consistent with the most recent growth rate calculations provided by *Fung and Viñas* [1994]. Partial wave reflection at the boundary is also included. A periodic boundary oscillation is introduced at the wall edge and the evolution of the AKR photons is monitored over numerous collisions with the wall. The concept is analogous to that applied to particle acceleration and is called Fermi acceleration via oscillating boundary. The system is described by a set of nonlinear coupled equations whose solutions can be either regular or choatic. Recently, a similar model was presented to explain the updrifting tones observed by Voyager at ELF frequencies in the heliospheric cavity [*Farrell*, 1993]. As will be demonstrated, very interesting phase space structure develops due to the AKR/boundary interaction.

Fermi Acceleration via Oscillating Boundary

Groundbreaking work on the study of Fermi acceleration of particles (with mass) via oscillating boundary was presented by *Ulam* [1961], who developed a numerical simulation of the process and found that particle motion could become stochastic, or randomized, in certain regions of phase space. An advanced, exact set of dynamically coupled equations describing particle motion in a cavity of any arbitrary size with an oscillatory boundary was presented by *Zaslavskii and Chirikov* [1965]. *Lichtenberg and Lieberman* [1983] refer to this set of equations as the "exact Ulam mapping." However, this complex set can be simplified if one assumes that the oscillating wall imparts momentum to the particle without changing position in space, which is approximately true if the oscillation displacement, $x(t)$, is much less than the size of the cavity, L: $x(t) \ll L$. In this case the set of coupled equations, often referred to as the "simplified Ulam mapping" reduces to [*Lichtenberg and Lieberman*, 1983]

$$u_{n+1} = |u_n + \sin \psi_n| \tag{1a}$$

$$\psi_{n+1} = \psi_n + \frac{2\pi M}{u_{n+1}} \tag{1b}$$

for a sinusoidal boundary oscillation, where u is the normalized particle velocity equal to v/V, v being the particle velocity, and V the boundary oscillation velocity; ψ is the phase of the wall oscillation; and $M = 2L/V\tau$. The index, n, represents the number of collisions with the wall. Results indicate that the u-ψ phase space is divided up into three separate regions: At low velocities ($u \ll M$) particle motion is almost completely randomized or stochastic; at intermediate velocities ($u \sim M$) regions of stochastic motion surround phase space "islands" of regular motion; and at high velocities ($u \gg M$) the motion is mostly regular. As a consequence of this structuring of phase space, particles initially injected at low velocities can be accelerated to higher velocities but must remain within the region where the motion is stochastic. They cannot enter the islands containing regular orbits.

Consider now the interaction of an extraordinary (X) mode radio photon of frequency ω propagating perpendicular to the ambient magnetic field in a field-aligned AKR density cavity of approximately 100 km size. The situation is illustrated in Figure 2. It is assumed that the AKR photon is generated in the cavity by a population of unstable, suprathermal electrons flowing along the local magnetic field.

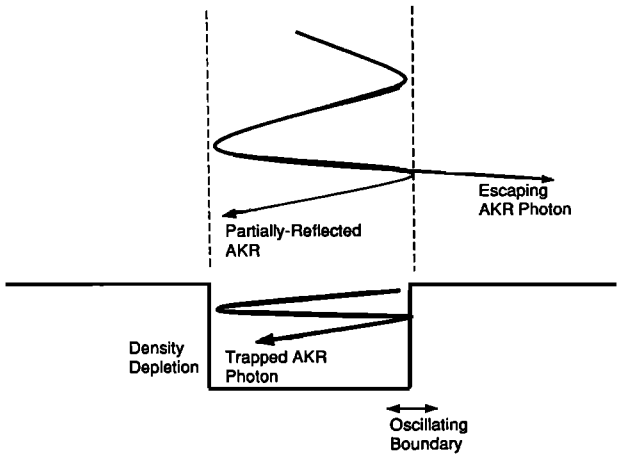

Figure 2. An illustration of the escaping and trapped AKR emission in an auroral plasma cavity.

Now assume that the cavity boundary possesses an oscillation of period τ. A mode possibly capable of creating such a perpendicular boundary oscillation is an electron plasma oscillation, which presumably could appear as a quasi-monochomatic "jitter" on the boundary near a frequency of 10 kHz. This possibility will be discussed further in a later section. The AKR radio photons propagate in the cavity at frequencies greater that the local X mode cutoff defined by $\omega_{ce}/2 + [(\omega_{ce}/2)^2 + \omega_{pe}^2]^{1/2}$ where ω_{ce} and ω_{pe} are the local electron cyclotron and plasma frequencies, respectively. In the cavity the AKR is amplified by as much as 70 dB [*Omidi et al.*, 1984] due to the cyclotron instability (i.e., the stimulated cyclotron emission process). At the edge of the cavity the wave will be partially reflected in association with the index of refraction mismatch at the boundary. Typically, the reflection is small, being only a few percent. However, wave trapping in the cavity will occur if the wave frequency lies below the X mode cutoff of the external region. In this case some emissions may mode couple to the outer regions via the Z mode, but such processes are not modeled here. Cases of wave escape and trapping are both illustrated in Figure 2.

The evolution of individual photons in the time-varying cavity can be modeled using a new set of nonlinear dynamically coupled equations that describe the Fermi acceleration of radio photons via an oscillating boundary. The equations are based upon the basic physical processes associated with the trapped photon: Doppler shifting at the oscillating boundary followed by wave dispersion in a plasma medium. Specifically, reflection from the oscillatory boundary will result in a Doppler shift in frequency of the radio photon, which can be expressed as

$$\omega_{n+1} = \omega_n \left[1 + \left(\frac{V}{c} \right) \left(\frac{c}{v_{p_n}} \right) \sin \psi_n \right] \tag{2a}$$

where ω is the wave frequency, V is the boundary oscillation velocity, v_p is the wave phase velocity, and ψ is the phase of the boundary oscillation. It is implicitly assumed that the boundary oscillation speed is relatively slow (i.e., $V/c \ll 1$) so that relativistic Doppler effects can neglected. Equation (2a) indicates that the Doppler-shifted frequency is equal to the original frequency plus a small perturbation. The strength of this perturbation is directly proportional to V/c, which can be considered the perturbation strength. This factor is parallel to the expansion factor used in classical perturbation theory [*Lichtenberg and Lieberman*, 1983]. In a dispersive medium, such as a plasma, the Doppler shift corresponds to a change in the radio photon group and phase velocities. Assuming an X mode emission propagating at large angles with respect to the ambient magnetic field, the group velocity, v_g, and phase velocity, v_p, can be easily derived from the corresponding electromagnetic dispersion equation. These quantities are

$$\frac{v_{g_{n+1}}}{c} = \frac{A}{A^2 + B^2 C} \tag{2b}$$

and

$$\frac{v_{p_{n+1}}}{c} = \frac{1}{A} \tag{2c}$$

where $A = (1 - B^2)^{1/2}$, $B = 1/(2\varepsilon - 1)$, $C = (\omega/\omega_{pe}) + \varepsilon$, and $\varepsilon = \omega(\omega - \omega_{ce})/\omega_{pe}^2$. It should be noted that quantity A is actually equal to the index of refraction for X mode signals and is the starting point for the derivations of (2b) and (2c). An identical equation for the index of refraction for the X mode was derived by *Calvert* [1982]. Finally, an equation similar to (1b) can be written to describe the phasing at the boundary after $n + 1$ reflections of the photon:

$$\psi_{n+1} = \psi_n + 2\pi M\left(\frac{c}{v_{g_{n+1}}}\right) \tag{2d}$$

where $M = 2L/c\tau$. The set (2a)–(2d) can be considered the "simplified Ulam mapping for radio photons" and holds true when the boundary oscillation displacement, $x(t)$, is much less than the scale size of the inhomogeneity, L.

The photons are partially reflected at the cavity boundary. In order to account for this energy loss from the cavity, the refection coefficient,

$$R = (\rho_1 - \rho_2)^2(\rho_1 + \rho_2)^2 \tag{3}$$

is calculated and tabulated after each of the n collisions. The quantities $\rho_{1,2}$ are the wave indices of refraction inside and outside the cavity, respectively. The wave growth of the photon through the 100-km-wide cavity was also determined using growth rate profiles determined by *Fung and Viñas* [1994]. Specifically, for a situation where f_{pe}/f_{ce} is equal to 0.2, the growth rate at relatively wide angles can be modeled as

$$\frac{\gamma}{f_{ce}} = 0.875\frac{f}{f_{ce}} - 0.916 \quad \text{for } 1.047 < \frac{f}{f_{ce}} < 1.055$$

$$\frac{\gamma}{f_{ce}} = -0.366\frac{f}{f_{ce}} + 0.393 \quad \text{for } 1.055 < \frac{f}{f_{ce}} < 1.070 \tag{4}$$

$$\frac{\gamma}{f_{ce}} = 0.0015 \quad \text{for } \frac{f}{f_{ce}} > 1.070$$

for a suprathermal loss cone distribution having a temperature of 2 keV (see Figure 5a of *Fung and Viñas* [1994]). The total wave power based upon partial wave reflection and wave amplification (via the cyclotron instability) in the cavity is determined for each of the n collisions and tabulated as a function of wave frequency. The transmitted power from the region is $(1 - R)\exp[2\gamma L/v_g]$.

An important property of the model is the dispersive magnetoplasma medium. In fact, if the medium were nondispersive, there would be no change in the velocity of information (i.e., the photon packet velocity, v_g) for photons of different frequency. As a result, the formation of "islands" of regular motion and stochastic regions would not occur, and the philosophical parallel of this model to the simplified Ulam mapping of particles would break down. It is the dispersive nature of the medium and the corresponding different group velocities that give rise to the interesting structure in phase space, including the formation of discrete frequency tones at resonant points.

Results

Figures 3a and 3b are typical examples of a frequency versus ψ phase space diagram, where ψ is the phase of the boundary oscillation defined in (2d). The diagram shows the AKR radio photon history at a specific point along the field-aligned density structure. In order to create a density cavity the local electron plasma-to-cyclotron frequency ratio in the generation region, f_{pe}/f_{ce}, is set to 0.2, while the region adjacent to the cavity was presumed to have an f_{pe}/f_{ce} ratio of 0.6. For the sake of demonstration the ratios have been preset to these values. One can imagine a near infinite set of values to test. To model the emission from this particular location, cyclotron emission is created by uniformly injecting 120 photons between the r-x cutoff value (near $f/f_{ce} = 1.042$) and $f/f_{ce} = 1.500$ into the system. The set of (2), (3), and (4) are iterated with 120 separate initial frequencies. The frequency/phase history of the 120 photons is recorded for 1000 collisions with the oscillating walls of the boundary. In this case the value of V/c, the speed of the boundary oscillation, is 0.025, and the value of M is set to 10 (Figure 3a) and 20 (Figure 3b). The frequency and phase of each photon after the nth collision is represented by an individual dot in the figure. The panel to the right in each figure is the sum total of the radiated power from the source point and represents the actual signal measured by a spacecraft.

As evident in each of the panels, an initially uniform emission becomes very complicated after numerous interactions with the oscillating boundary. Initially, the signal was of constant value, being of equal amplitude from $f/f_{ce} = 1.042$ to $f/f_{ce} = 1.500$. However, emissions below about $f/f_{ce} = 1.28$ cannot escape the cavity due to the higher r-x cutoff frequency in the adjacent region outside the cavity. These emissions remaining trapped within the cavity may possibly convert to Z mode at the boundary.

At frequencies above $1.28 f_{ce}$ both discrete tones and a stochastic background emission are formed from the interaction of the radio photons with the

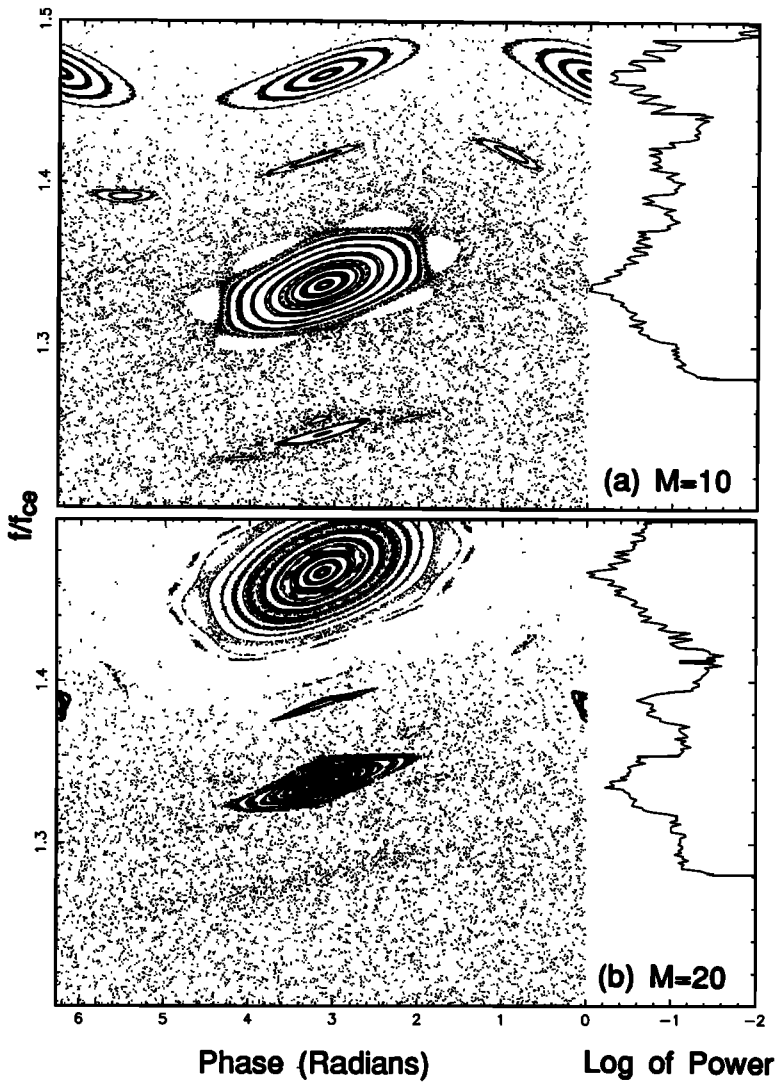

Figure 3. The phase space history of photons following 1000 collisions with an oscillating boundary, with the perturbation factor, V/c, set to 0.025 and M set to (a) 10 and (b) 20. The f_{pe}/f_{ce} ratio in the cavity is set to 0.2, while that outside is 0.6. The panels to the right show the total radiated power including both reflection and wave amplification in the source region. Note that discrete emission is associated with the resonance island structures.

boundary. Most of the photons interact with the oscillating boundary in a stochastic or chaotic way, forming the background. The location of such photons in phase space is highly variable and appears almost random. However, the motion is still deterministic, being define by the set (2), (3), and (4). This situation is usually referred to as deterministic chaos. As an example, we have plotted the time history of a stochastic-type photon in Figure 4a, this being the photon at a frequency of 1.50 f_{ce} from Figure 3a. Note that the photon phase is highly variable, but there is a statistical tendency for the photon to downshift in frequency. This downshifting occurs because the Doppler shift term in (2a) is itself a function of frequency (for $\omega \gg 0$, $\Delta\omega \propto \omega$) which makes the photon trajectory in phase space irreversible: Two successive collisions of equal but opposite value will place the photon at a lower frequency than its initial value. For example, if a photon of frequency ω_0 is incident on the boundary

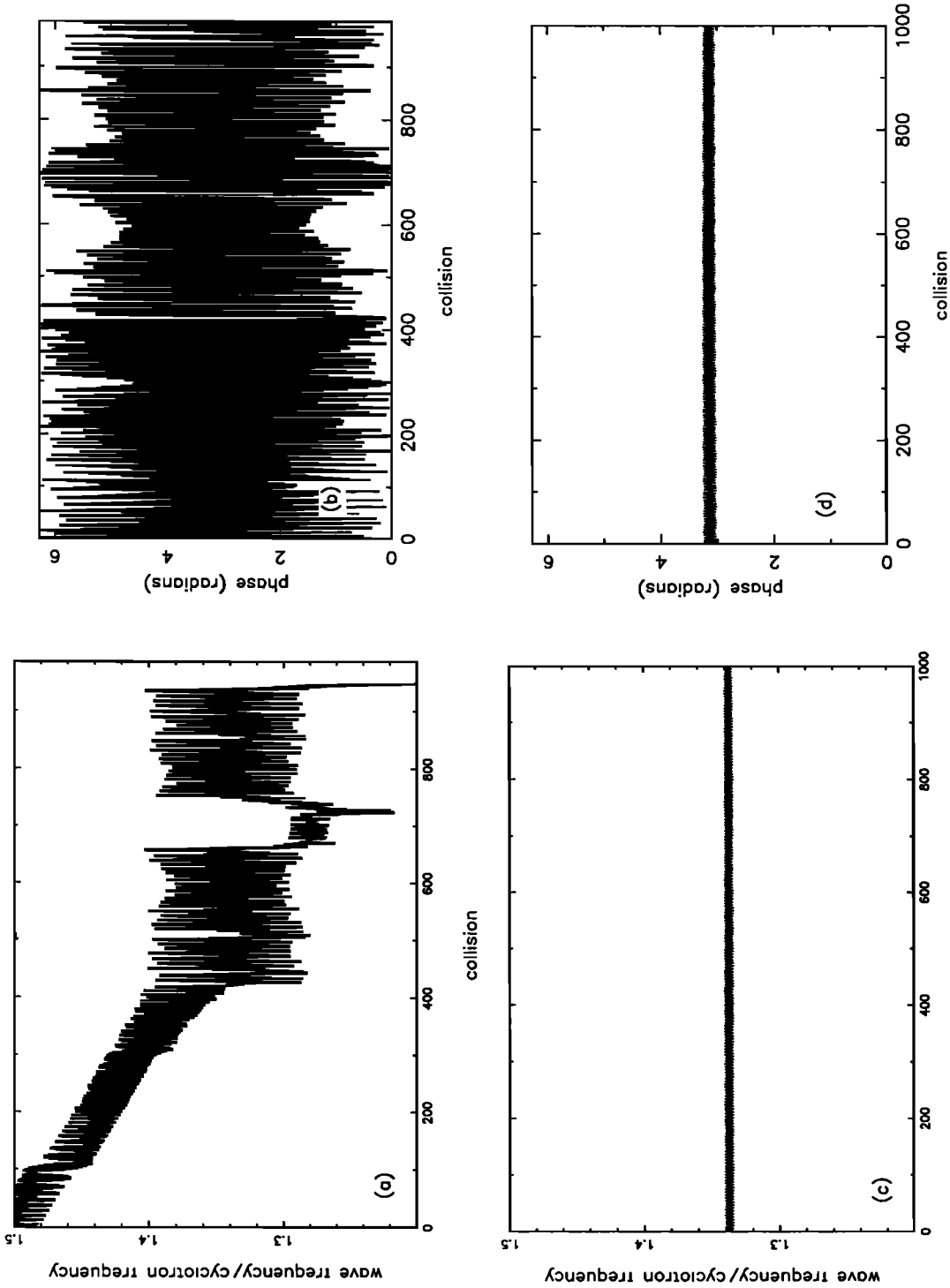

Figure 4. The collision history for two photons with a boundary with $V/c = 0.025$ and $M = 10$. The f_{pe}/f_{ce} ratio in the cavity is set to 0.2, while that outside is 0.6. Shown are the (a) frequency and (b) phase history for a photon whose initial frequency is $1.5 f_{ce}$. This photon is not in resonance with the boundary, and thus possesses nearly random phase. In contrast, the (c) frequency and (d) phase history for a photon near $1.334 f_{ce}$ are shown. This photon is in resonance with the boundary, and thus the frequency and phase remain nearly constant throughout its lifetime.

moving inward at $+V$, the Doppler shift is $\Delta\omega_{up} \sim +\omega_0 V/c$. If it next hits the wall moving outward at the same velocity (i.e., $-V$), the Doppler shift is $\Delta\omega_{down} \sim -(\omega_0 + \Delta\omega_{up})V/c$. The net shift following both these collisions is, however, not zero, but $\Delta\omega_{total} \sim -\omega_0(V/c)^2$, with the photon now at a lower frequency than initially started even though the wall velocities were of equal but opposite values. Using similar arguments, it can also be shown that reversing the order of the collisions still yields a net downward shifted photon. Consequently, after numerous random collisions with the boundary the photons will systematically drift downward in frequency in this region of phase space.

Of considerable interest is the region of phase space where the Doppler shifting creates regular (i.e., nonstochastic) photon trajectories. In this case "islands" in phase space are created where the photon motion remains localized in frequency. Photons trapped in these regions cannot escape, and remained localized for their lifetime to the limited frequency extent. These regular islands are centered at resonant points, where the transit time between collisions, T, is an integer ratio of the boundary oscillation period, τ (i.e., $\pi/T = j/k$). Such a condition is common for resonance [*Lichtenberg and Lieberman*, 1983]. For example, in Figure 3a, the relatively large circular region centered at 1.34 f_{ce} corresponds to a resonance of photon transit time with eleven boundary oscillations (i.e., $v_g/cM = \pi/T = 1/11$). The resonant photons within the island regions map out regular, circular patterns like those seen surrounding the resonant point at $1.34 f_{ce}$. A photon starting on one of these circular patterns will remain on the pattern. Resonant photons cannot extend into the stochastic region and frequency shift in a random way. Because the resonant photon remains relatively localized in phase space, wave intensification occurs at the associated frequencies, thereby creating the narrowbanded tones. The calculated power including reflection and wave growth (i.e., the panel to the right in each figure) indicates an enhancement in wave energy near the resonant points, this being detected by the spacecraft as wave intensification above background levels. Figure 4b shows the phase space history of a photon at $1.334 f_{ce}$ found in Figure 3a, the photon being trapped in a regular region. Note that the photon remains at nearly the same frequency and phase for its lifetime.

At this point we have demonstrated how an emission can become discrete and structured via the Fermi acceleration process. However, observations like those of Figure 1 suggest that the tones also uniformly drift in frequency. In the Fermi acceleration process, such a drift is possible by adiabatically varying the parameter M, which is proportional to L/τ. Thus a slow change in the size of the density structure or a slow change in the boundary oscillation period will create an updrift or downdrift to the signals. As an example, a spectrogram is shown in Figure 5 which displays the evolution of the tones in frequency as a function of M. Note that as M increases, the tones updrift in frequency. If M decreases, the same tones would appear to downdrift. Also, note that the slope of the drift is different for each tone, and this slope is nonuniform as a function of M. It appears that the variation of the set of tones as a function of M is not linear. The appearance of the tones is very similar to those shown in Figure 1.

Discussion

A critical element to the Fermi acceleration model as applied to the AKR is the identification of the boundary oscillation (i.e., the mode responsible for the boundary oscillation). Given a value of M = 5–20 and a local cavity size of 100 km, the boundary oscillation period required for the development of the observed tones is about 10^{-4} s. Such values correspond to a boundary frequency of about 10–20 kHz. Figure 6 shows a radio spectrum obtained by the Viking spacecraft in the auroral region at the generation location of the AKR [*Perraut et al.*, 1990]. The measurements reveal the presence of a distinct peak near the local electron plasma frequency (labeled in the figure as f_{pe}), this occurring in the tens of kilohertz regime. Auroral hiss is observed at frequencies below f_{pe}. Spin phase analysis reveals that the natural f_{pe} emission is highly directional, propagating nearly quasi-parallel to the local magnetic field. Density variations associated with this electrostatic emission should develop in a direction perpendicular to the field-aligned density depletion, and these could act as the boundary oscillation responsible for the discrete AKR tones. The geometry of the situation is illustrated in Figure 7. Thus it appears that the creation of distinct tones in the AKR is possible with the associated development of a strong emission at the local electron plasma frequency.

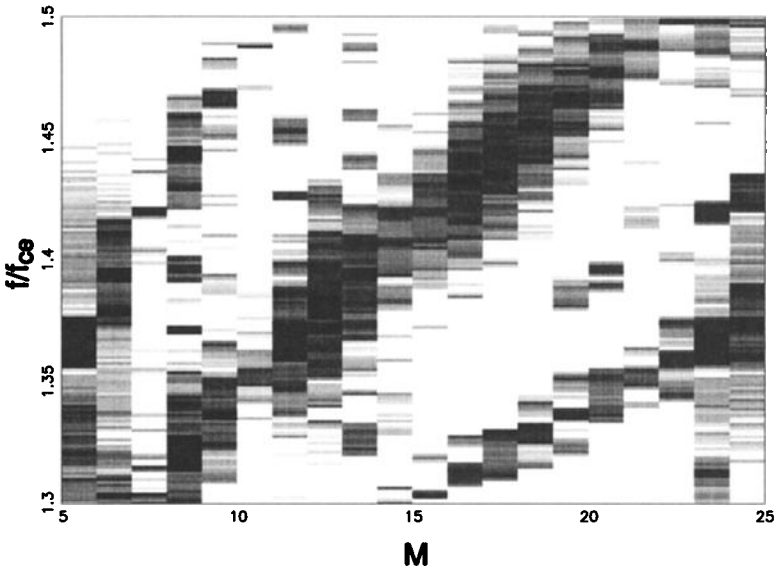

Figure 5. A frequency-versus-M spectrogram for V/c set to 0.025. The f_{pe}/f_{ce} ratio in the cavity is set to 0.2, while that outside is 0.6. The dark regions represent the strongest emitted powers. Note that as M slowly increases, the frequency of the discrete structure (i.e., intensified signal shown in black) updrifts.

It should be noted that the local cavity of 100 km extent is a structure much smaller than the "auroral plasma cavity" originally described by *Calvert* [1981b]. The former is a local density perturbation, while the latter refers to a large density depletion over the nightside auroral zone. In this model we assume the smaller density perturbation actually lies within the larger depleted region referred to as the auroral plasma cavity.

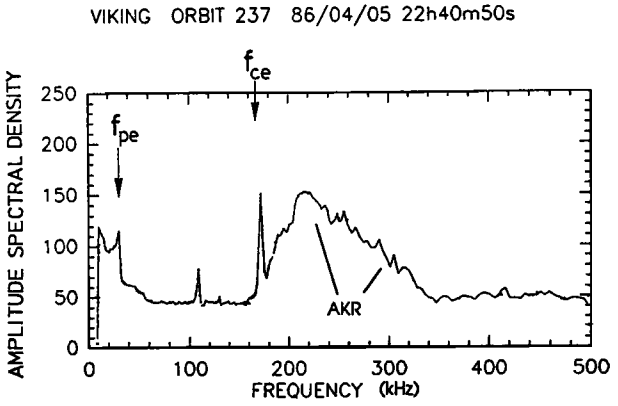

Figure 6. The radio spectra obtained by Viking in the AKR source region. Note the presence of a strong emission near the local plasma frequency, f_{pe}. Adapted from *Perraut et al.* [1990].

As indicated in Figure 3, the discrete tones lie on top of a more diffuse AKR background created by the stochastic photons. These tones are typically about 10–20 dB above the diffuse background level. The presence in the model of both a diffuse and discrete AKR component is consistent with observation. Conflicting evidence on the nature of AKR was described by *Kaiser* [1990]. Specifically, wideband waveform receivers of limited instantaneous dynamic range indicate that AKR consists of many sets of discrete tones. Figure 1 is a good example. Based on this figure and others like them, it is easy interpret the images of AKR structure as consisting of discrete tones only, without any background activity in between the tones. However, this conclusion is deceiving. Specifically, the amplitude measurement windows of waveform receivers is set by an automatic gain control system that places the low-intensity edge of measurement window near the largest average value. Consequently, discrete structures like tones and isolated emission bursts are easily observed, while a diffuse, continuous background emission will go undetected (since the diffuse background sets the low end sensitivity of the receiver). Thus with an automatic gain control (AGC) system one may be observing only the "jagged tips" of a large iceberg. In contrast, spec-

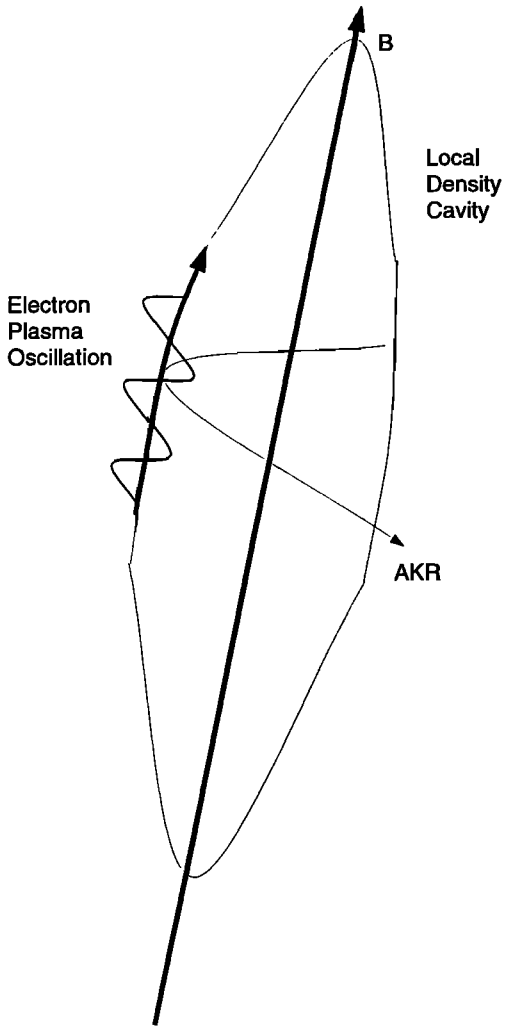

Figure 7. An illustration of the electrostatic/electromagnetic wave mode interaction in the local cavity.

trum analyzer measurements (with large dynamic range over a large frequency band and large time width) suggests that AKR is correlated over many hundreds of kilohertz. Such an observation is consistent with the presence of a continuous, smooth emission. This apparent observational inconsistency can be accounted for if AKR has both a discrete and a diffuse nature.

Observations presented by *Morioka et al.* [1981] indicate that AKR does indeed possess both a discrete and diffuse nature. Specifically, the high resolution/fast sampling receiver flown on Exos B has enhanced dynamic range (60 dB) over typical waveform receivers, but also has high spectral resolution. Their Figure 13 indicates that AKR consists of a diffuse background component lying nearly 40 dB above the receiver floor. Superimposed on the diffuse component are discrete tones raised about 10 dB above the smooth background. There is in fact a distinct similarity between Morioka et al.'s observations and the model results presented here. Unlike most models of the AKR fine structure, the one presented here predicts the presence both types of AKR emission: the discrete and diffuse components.

The effect of varying the parameter M is shown in Figures 3 and 5. As is evident, changing M results in the frequency drift of the resonance islands. This effect occurs because a change in M (i.e., change cavity size or boundary oscillation frequency) alters the resonance condition, $v_g(f_{res})/cM = j/k$, thus requiring a new population of photons at a different frequency and light travel time to be in phase with the boundary oscillation. Thus the parameter M is critical in determining the frequency of the discrete tones.

The effect of varying the perturbation strength, V/c, is to define the tone bandwidth. The frequency location of the resonant islands is determined solely by M, but the strength of the resonance, or the size of the islands in frequency, is determined by V/c. As V/c decreases, the size of the resonance islands (or the number of photons in resonance) decreases. As V/c goes to zero the islands disappear altogether, removing the tones and leaving the original undisturbed broadband emission. Thus the value of V/c does not determine the resonance frequency, but rather the bandwidth of the tone.

In the simulation it is assumed a priori that the emission is generated in a local density cavity. As such, only the higher frequency drifting tones are able to escape the source region and propagate freely into the surrounding high-density plasma. However, it is worthy to investigate the situation where the AKR is generated in a density enhancement. In this new case all emission from the r-x cutoff frequency upwards is able to escape the active source region. The region of largest wave growth lies just above the local r-x cutoff in the source [*Omidi et al.*, 1984; *Fung and Viñas*, 1994], and this region of enhanced emission tends to dominate the spectrum. Figure 8 shows the collision history of 120 photons after 1000 collisions with a wall of $V/c = 0.025$ and $M = 10$, with $f_{pe}/f_{ce} = 0.2$ inside the source region but $f_{pe}/f_{ce} = 0.1$ outside the

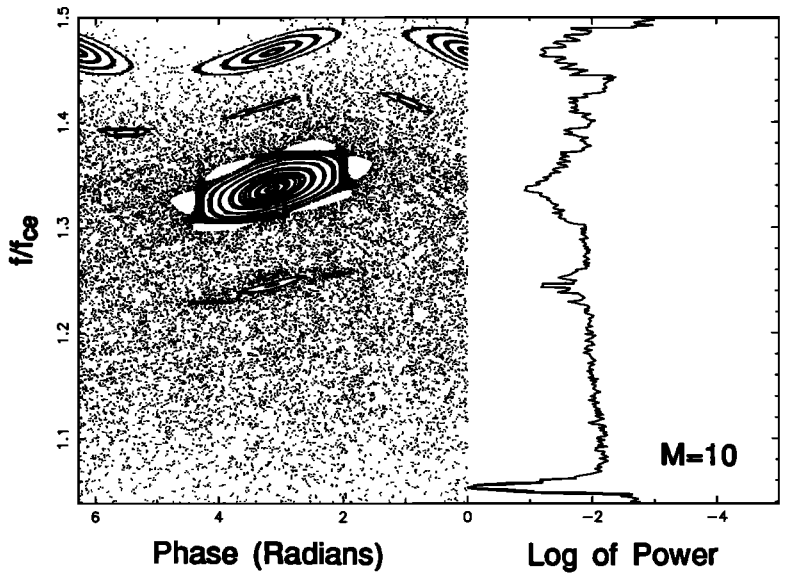

Figure 8. The phase space history of photons following 1000 collisions with an oscillating boundary, with the perturbation factor, V/c, set to 0.025 and M set to 10. The f_{pe}/f_{ce} ratio in the active region is set to 0.2, while that outside is 0.1 (i.e., a density enhancement). Note that the largest intensities are associated with the region of largest growth rate lying just above the r-x cutoff frequency.

source region. The situation is identical to that of Figure 3a except for the lowered plasma frequency outside the source region. As evident in the figure, emission at all frequencies can escape. Most notable is the fact that emissions at lower frequencies, in the large wave growth region, dominate the spectra, lying nearly 20 dB above the intensity level associated with the resonant islands. Figure 9 shows a frequency M spectrogram like that of Figure 4, only now having $f_{pe}/f_{ce} = 0.1$ outside the source region. Note that emissions generated in the large growth rate region dominate the spectra. It is concluded that Fermi acceleration model is most consistent with the observation of drifting tones only if the emission is generated in density cavities. In other words, Figure 5 is a better representation of the emission than Figure 9; thus the model represents reality in a local cavity generation region.

The Fermi acceleration model for AKR fine structure involves numerous collisions with a moving boundary. At each collision, a fraction of the wave energy will be converted to O mode emission in a way consistent with the electromagnetic boundary conditions. The exact amount of O mode emission has not been calculated in the simple model presented here. However, the efficiency of the conversion process should improve as frequency increases, due to the converging values of the O and X mode indices of refractions. As such, the model may also explain some or all of the observed O mode emission observed from the AKR source region. This statement is made in a general way here, leaving quantification for future work.

The model presented is two-dimensional in nature, describing AKR emission propagating quasi-perpendicular to the local magnetic field. Despite the obvious drawbacks of such a system, the model is relevant for the problem since cyclotron emission is typically beamed at large angles with respect to the local magnetic field. Further, the Viking observations of the discrete f_{pe} emission indicate that a real quasi-perpendicular boundary oscillation may be present at the edge of the density structures. Thus modeling the activity in the azimuthal plane about the auroral field line is a legitimate approach in understanding the basic physical process of discrete tone formation.

Conclusion

It is demonstrated that Fermi acceleration of radio photons can account for the fine structure

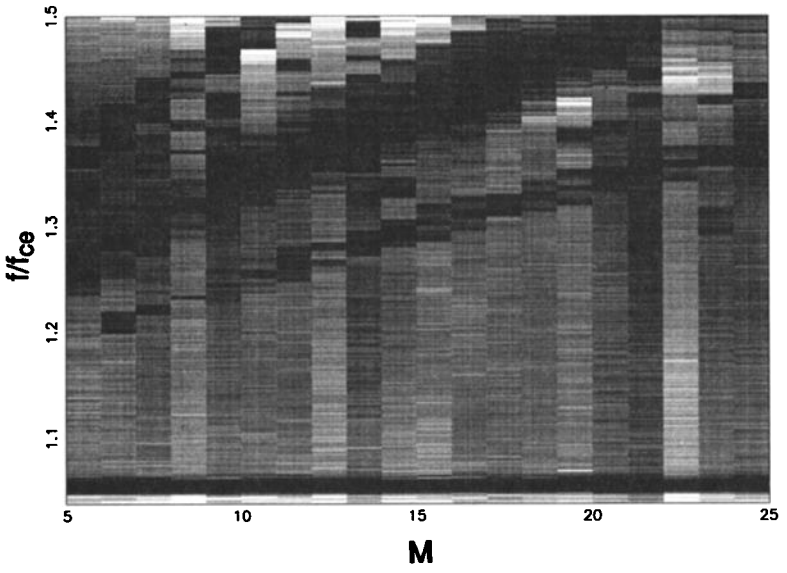

Figure 9. A frequency-versus-M spectrogram, similar to that of Figure 5, for V/c set to 0.025. The f_{pe}/f_{ce} ratio in the cavity is set to 0.2, while that outside is now set to 0.1 (i.e., a density enhancement). Again, note that the largest intensities are associated with the region of largest growth rate lying just above the r-x cutoff frequency.

observed with the auroral kilometric radiation. An active region generating relatively diffuse cyclotron emission can be the source of intense discrete tones if a boundary oscillation is present at the edge of the density structure associated with the wave generation region. The boundary oscillation forms a resonance with the reflected photons, creating both stochastic and regular photon trajectories. The stochastically scattered photons generate a diffuse background radiation level while the regular photon trajectories create the more intense discrete tones. Assuming that there are a number of active sites along the field-aligned density cavity where AKR is generated, then numerous sets of tones are possible, giving rise to the complicated spectral structure of AKR.

Electron plasma emission propagating along the field line, like that observed by Viking, could be the boundary oscillation responsible for the activity. In this case the coupling of radio and plasma waves is nonlinear. The emission is still assumed to be generated directly by the cyclotron resonance process like that described by *Wu and Lee* [1979]. However, the formation of discrete tones is caused by the nonlinear radio/plasma wave coupling occurring at the boundary of the AKR source region.

In general, there may be many possible applications of the theory involving Fermi acceleration of radio photons. Any emission fully or partially trapped in a region can have its spectral structure altered via the resonance process with the oscillating boundary. A recent application of this model was the explanation of structure associated with the heliospheric cavity emission [*Farrell*, 1993]. Other potential applications include explaining unusual trapped emissions generated by spacecraft sounders, the formation of discrete tones in trapped terrestrial and Jovian continuum emission, etc.

Acknowledgments. I would like to thank A. F. Vinas for very informative conversations and encouragement. M. L. Kaiser and M. D. Desch are both thanked for their reviews and encouragement with regard to this work. I would like to especially thank Dwight Nicholson, who introduced me to the topic of stochasticity and nonlinear dynamics.

References

Baumback, M. M., and W. Calvert, The minimum bandwidths of auroral kilometric radiation, *Geophys. Res. Lett.*, *14*, 119, 1987.

Benson, R. F., W. Calvert, and D. M. Klumpar, Simultaneous wave and particle observations in the auroral kilometric source region, *Geophys. Res. Lett.*, *7*, 959, 1980.

Calvert, W., A theory for the auroral kilometric and

Jovian decametric radiation cones, *Res. Rep. 81-6*, Univ. of Iowa, Iowa City, 1981a.

Calvert, W., The auroral plasma cavity, *Geophys. Res. Lett.*, *8*, 919, 1981b.

Calvert, W., A feedback model for the source of auroral kilometric radiation, *J. Geophys. Res.*, *87*, 8199, 1982.

Dunckel, N., B. Ficklin, L. Rorden, and R. A. Helliwell, Low-frequency noise observed in the distant magnetosphere with OGO 1, *J. Geophys. Res.*, *75*, 1854, 1970.

Farrell, W. M., The heliospheric cavity radio emission: Generation of discrete tones by Fermi acceleration via oscillating boundary, *Geophys. Res. Lett.*, *20*, 2011, 1993.

Farrell, W. M., and D. A. Gurnett, The statistical study of solar Type III bursts and auroral kilometric radiation onsets, *J. Geophys. Res.*, *90*, 9634, 1985.

Farrell, W. M., W. Calvert, and D. A. Gurnett, AKR signal increases caused by triggering, *Geophys. Res. Lett.*, *13*, 370, 1986.

Fung, S. F., and A. F. Viñas, Excitation of high-frequency electromagnetic waves by relativistic electrons with a loss cone distribution in a field-aligned potential drop, *J. Geophys. Res.*, *99*, 8671, 1994.

Gallagher, D. L., and D. A. Gurnett, Auroral kilometric radiation: Time-averaged source location, *J. Geophys. Res.*, *84*, 6501, 1979.

Gurnett, D. A., The Earth as a radio source: Terrestrial kilometric radiation, *J. Geophys. Res.*, *79*, 4227, 1974.

Gurnett, D. A., and R. R. Anderson, The kilometric radio emission spectrum: Relationship to auroral acceleration processes, in *Physics of Auroral Arc Formation* Geophys. Monogr. Ser., vol. 25, edited by S.-I. Akasofu and J. R. Kan, pp. 341–350, AGU, Washington, D. C., 1981.

Gurnett, D. A., R. R. Anderson, F. L. Scarf, R. W. Fredricks, and E. J. Smith, Initial results for the ISEE 1 and 2 plasma wave investigations, *Space Sci. Rev.*, *23*, 103, 1979.

Huff, R. L., W. Calvert, J. D. Craven, L. A. Frank, and D. A. Gurnett, Mapping of auroral kilometric radiation sources to the aurora, *J. Geophys. Res.*, *93*, 11,455, 1988.

Kaiser, M. L., Fine structure of planetary radio emissions (abstract), *Eos Trans. AGU*, *17*, 596, 1990.

Kaiser, M. L., and J. K. Alexander, Relationship between auroral substorms and the occurrence of terrestrial kilometric radiation, *J. Geophys. Res.*, *82*, 5283, 1977.

Lichtenberg, A. J., and M. A. Lieberman, *Regular and Stochastic Motion*, Springer-Verlag, New York, 1983.

Louarn, P., A. Roux, H. de Feraudy, D. Le Queau, M. Andre, and L. Matson, Trapped electrons as a free energy source for the auroral kilometric radiation, *J. Geophys. Res.*, *95*, 5983, 1990.

McKean, M. E., and R. M. Winglee, A model for the frequency fine structure of auroral kilometric radiation, *J. Geophys. Res.*, *96*, 21,055, 1991.

Melrose, D. B., An interpretation of Jupiter's decametric radiation and the terrestrial kilometric radiation as direct amplified gyroemission, *Astrophys. J.*, *207*, 651, 1976.

Melrose, D. B., A phase-bunching mechanism for fine structure in auroral kilometric radiation and Jovian decametric radiation, *J. Geophys. Res.*, *91*, 7970, 1986.

Morioka, A., H. Oya, and S. Miyatake, Terrestrial kilometric radiation observed by Satellite Jikiken (EXOS-B), *J. Geomagn. Geoelectr.*, *33*, 37, 1981.

Omidi, N., and D. A. Gurnett, Growth rate calculations of auroral kilometric radiation using the relativistic resonance condition, *J. Geophys. Res.*, *87*, 2377, 1982.

Omidi, N., C. S. Wu, and D. A. Gurnett, Generation of auroral kilometric radiation and *Z* mode radiation by the cyclotron maser mechanism, *J. Geophys. Res.*, *89*, 883, 1984.

Perraut, S., H. de Feraudy, A. Roux, P. M. E. Decreau, J. Paris, and L. Matson, Density measurements in key regions of the Earth's magnetosphere: Cusp and auroral region, *J. Geophys. Res.*, *95*, 5997, 1990.

Pritchett, P. L., and R. M. Winglee, Generation and propagation of kilometric radiation in the auroral plasma cavity, *J. Geophys. Res.*, *94*, 129, 1989.

Ulam, S., *Proc. 4th Berkeley Symp. Math. Stat. Probab.*, *3*, 315, 1961.

Wu, C. S., and L. C. Lee, A theory of the terrestrial kilometric radiation, *Astrophys. J.*, *230*, 621, 1979.

Zaslavshii, G. M., and B. V. Chirikov, Fermi acceleration mechanism in the one-dimensional case, *Sov. Phys. Dokl., Engl. Transl.*, *9*, 989, 1965.

W. M. Farrell, Laboratory for Extraterrestrial Physics, NASA Goddard Space Flight Center, Code 695, Greenbelt, MD 20771. (e-mail: farrell@lepwmf.gsfc.nasa.gov)

(Received July 12, 1994; revised February 17, 1995; accepted February 23, 1995.)